Tuijin Jishu/Journal of Propulsion Technology
ISSN: 1001-4055
Vol. 46 No. 04 (2025)

Improved Global Positioning System Receiver using Extended Kalman filter with Hybrid Optimization

[1*]N V Maheswara Rao, [2] V.B.S. Srilatha Indira Dutt, [3] B.T. Krishna

[1]Assistant professor, Dept of ECE, Gayatri Vidhya Parishad College of Engineering for Women, Visakhapatnam, India*

[2]Professor, Dept of ECE, GITAM UNIVERSITY, Visakhapatnam, India

[3]Professor, Dept of ECE, University College of Engineering, JNTUK, Kakinada, Andhra Pradesh, India

[1]Corresponding author email id: himahesh4u@gmail.com*

Abstract

For precise timing, positioning, and navigation in a variety of applications, Global Navigation Satellite Systems (GNSS) are crucial. However, adverse conditions including dynamic movement, variable noise statistics, and poor signal reception might make GNSS signal tracking problematic. To mitigate these challenges, the research proposes the adaptive Weighted Strong Extended Kalman Filter as a possible means of enhancing GNSS receiver tracking performance. The approach dynamically optimizes the Kalman filter parameters to improve the accuracy of GNSS receivers in dynamic environments. Setting up the Kalman filter's required parameters, such as the measurement noise covariance, process noise covariance, state covariance matrix, and starting state estimations, is the first stage of the study. This algorithm uses "Chimphopper Hybrid Optimization (ChHO)," a novel hybrid optimization technique, to improve receiver positional accuracy. The proposed hybrid optimization algorithm creates a powerful framework for GNSS receiver performance optimization by building on the benefits of the popular Grasshopper optimization algorithm (GOA) and Chimp optimization algorithm (ChoA). This presents a novel approach that blends cutting-edge optimization approaches with conventional Kalman filter techniques to enhance GNSS receiver positioning capabilities which result in more reliable and resilient GNSS receiver systems.

Keywords: *GNSS, Adaptive Weighted Extended Kalman Filter, Chimphopper Hybrid Optimization, Positional accuracy.*

1. Introduction

GNSS uses range radio-frequency signals to produce a real-time position estimation, it has become an essential tool in today's world [1]. These days, GNSS is utilized for a variety of applications, including precise timing in agriculture and finance, scientific applications like geodesy and surveying, and safety-critical applications like maritime navigation and aviation. GNSS depends on signals from a collection of satellites orbiting the planet, but adverse conditions and shifting conditions can interfere with these signals [2]. Weak signal strength, unpredictable motion, and varying noise levels are just a few of the challenges GNSS receivers must deal with. The so-called tracking stage of GNSS receivers is responsible for one of their primary functions, which is signal tracking [3]. The carrier tracking loop, one of the most crucial components of a GNSS receiver, has a threshold that sets the maximum unassisted receiver performance and makes it exceedingly brittle in low signal situations. For precise synchronization in the majority of communication or satellite navigation domains, carrier tracking is essential [4]. Aligning with the time-varying dynamic propagation impacts on the carrier signals in the presence of potential interferences and channel noise is the main goal of carrier tracking. This serves as the foundation for users to

retrieve hidden information sent via channel links. Unexpected performance declines and distinct error residuals will result from the miss alignment [5].

An extremely crucial component of the GNSS receivers is the carrier tracking loop, which synchronizes the local carrier with the incoming signals [6]. The carrier tracking loop frequently uses the phase lock loop (PLL), however it is very delicate, especially in hostile surroundings [7]. The Kalman filter (KF) has been incorporated into the tracking loop to provide resilient tracking and improve tracking performance in challenging environments. Numerous studies have demonstrated that, in challenging circumstances, KF-based tracking performs better than PLL tracking. But accurate understanding of the system, noise statistics, and measurement models are crucial to KF's performance [8]. However, it is challenging to determine precise models and noise statistics because of the intricate situation within the tracking system. The noise covariances in KF-based tracking are initialized prior to iteration and stay constant throughout the filtering procedure [9]. Nevertheless, the static noise covariances cannot capture the actual conditions when the external environment is changing. It is challenging for KF tracking to keep up with these changes quickly or to get the best estimates under variable conditions [10].

The Extended Strong Adaptive Kalman Filter (ESTKF) is an advanced variant of the Kalman Filter (KF) that is well-known for improving robustness against model errors and mismatches in system parameters, especially in dynamic and evolving systems. It is widely used in inertial navigation systems that are integrated because it can greatly enhance navigation integration processing. [11]. Although KF works well in many situations, when faced with erroneous models, it might not always function at its best. This restriction results from the KF algorithm's built-in decision rules, which occasionally produce false alarms (incorrect detections) or fail to activate when they ought to (missed detections) [12]. Therefore, it is acknowledged that filter needs to be improved even more, especially when it comes to the carrier tracking system of GNSS receivers in difficult environments. To effectively handle mismatched models, these demanding environments may introduce a variety of uncertainties and inaccuracies, necessitating the use of more clever and adaptable strategies [13]. In order to ensure that KF can function optimally even in situations where traditional filter may not be able to handle the complexities of GNSS tracking and navigation, researchers and developers are investigating ways to make KF more intelligent and adaptable [14]. Hence, compared to KF tracking and KF tracking, ESTKF tracking can accomplish improved tracking accuracy under fragile and fluctuating signal circumstances [15].

The major contribution of this work are as follows:

- The work presents an algorithm for improving GPS receiver performance.
- To incorporate hybrid optimization algorithms and the weighted parameters are added to update the Kalman gain for better position accuracy.
- To increase the accuracy of the process noise covarience(Q_k) and measurement noise covariance (R_k) is tuned using the Chimphopper Hybrid Optimization (CHHO).
- To obtain the optimal solution, the location of the agent is updated on the basis of the gravitational force of the grasshopper behaviour.

The paper is organised as follows: Section 2 explains the related works of existing methods. The proposed methodology is described in the section 3. The outcomes and analysis are done in the Section 4. Section 5 ends with the conclusion.

2. Literature Review

"Some of the recent research works related to GNSS receiver tracking were reviewed in this section"

In 2022, Sun, B., *et al* [16] have suggested an integrated navigation algorithm that utilizes a multiple fading factors (MFKF) to handle the issues that the KF algorithm simply caused diffusion when the model became unreliable or noisy, and the MFKF precision was decreased when the fading factor was overused. The algorithm created a better basis for evaluating filtering anomalies depend on the novel covariance and changed the filtering state to more appropriately time the onset of the fading factor.

In 2019, Yue, Z., *et al* [17] have proposed a newly developed, robust SCKF. The computational complexity was decreased by the proposed algorithm's use of the measurement update module utilizing singular value decomposition (SVD). The orthogonality of the innovation was also used to derive a novel method for obtaining a suboptimal fading factor that was easy to compute and didn't require the Jacobian matrix to be solved. This new technique square-rooted the state prediction covariance matrix and added the calculated suboptimal fading factor. The algorithm became more robust when the process model was uncertain because the gain matrix could then be changed online.

In 2021, Pan, C., *et al* [18] have developed a tightly coupled GNSS/MIMU integration using two GNSS antennas, and according to the integration's model characteristics, suggested a singular value decomposition (SVD)-based robust adaptive cubature KF (SVD-RACKF). In order to extract the carrier's high-accuracy heading angle, two antennas were employed in this combination. The observation used to constrain the filtering estimation was the current attitude angle data. The mathematical accuracy of the recursive filtering was stabilized by using SVD in the suggested SVD-RACKF.

In 2019, Lou, T.S., *et al* [19] have suggested a brand-new partially strong tracking extended consider KF (PSTECKF). The introduced PSTECKF algorithm did not estimate the biases, but rather used a nonlinear "consider" approach to add their covariance and co-covariance to the covariance of the state estimation. Apart from the co-covariance between the biases and states, the PSTECKF also partly integrated an adaptive fading factor into the expected covariance of the states to adjust for the nonlinear approximation errors and navigation system covariance uncertainties.

In 2022, Shen, C., *et al* [20] have introduced a newly developed adaptive KF for nonlinear combined schemes. For an integrated navigation system that uses the MEMS-INS, GPS, and polarization compass, they suggested an enhanced “multi-rate strong tracking square-Root cubature KF (MR-STSCKF)”. The system covariance was adaptively estimated using the proposed filter. They suggested a method that would solve the issue of inconsistent sampling rates across various sensors while preserving the high accuracy of integrated navigation results.

In 2020, Liu, S., *et al* [21] have suggested estimating C/N0 using the ASTKF. Through static field test and simulation experiments, the estimator was assessed. The findings showed that the method could accurately estimate the weak signal C/N0 and that the ASTKF C/N0 estimator could pursue sudden disparities in C/N0. The ASTKF estimation approach outperformed the AKF technique the amount of time that passed after C/N0 jumped.

In 2021, Mu, R. and Long, T. [22] have suggested a VTL implementation framework that could be executed with only minor adjustments on a current receiver platform. A partial transparent numerically controlled oscillator (NCO) control mode serves as its foundation. The authors provided a detailed introduction to the architecture of VTL, the navigation filter's design, and the key elements of hardware configuration. Lastly, a GPS simulator test was used to confirm the VTL's performance. The outcomes demonstrated that the suggested VTL could function in real-time and that it was significantly more effective at maintaining the tracking of high-dynamic signals.

In 2021, Gao, B., *et al* [23] have suggested a fresh approach to the issue of GNSS/INS integration that is tightly coupled. The Mahalanobis distance concept was used to thoroughly derive a new strong CKF with resulting memory for observations modelling error and an innovative adaptive CKF with fading memory for dynamic modelling error, without even the use of artificial empiricism. Based on this, the standard, adaptive and robust CKF results were combined using the interacting multiple model (IMM) principle to create a new CKF that has both robustness and adaptability.

In 2021, Cheng, L., *et al* [24] have suggested a novel assisted structure in which LEO Doppler positioning helped with GNSS signal collection and Doppler tracking. For the initial Doppler positioning, the receiver used the LEO signal. Then, to aid in the acquisition and tracking of GNSS, the coarse position with the GNSS navigation communications gathered from LEO and the predictable clock data were used. This integrated system may enhance the sensitivity of the GNSS receiver. The organisation of the assisted receiver was presented, and a thorough analysis of the carrier tracking performance and assisted GNSS acquisition of signals was done.

In 2022, Klokov, A., *et al* [25] have suggested a novel Gauss-Hermite KF-based carrier tracking algorithm for stationary and mobile recipients with weak GPS signals in their paper. The algorithm was created to function when receiving a dynamic and unreliable GPS signal. In their approach, they took into account a technique for generating joint estimates of the RNP in a intelligible tracking mode. A software-defined simulator and an SDR device were used to simulate the algorithm's performance and assess it. EKF and UKE were tested as two additional nonlinear tracking algorithms for comparison.

2.1. Problem statement

The main issue is that accurate and dependable GNSS tracking is required to meet a variety of real-world obstacles. Weak signal conditions, dynamic movement, noisy environments, unreliable models, and sudden changes in signal quality (C/N0) are some of the factors that can affect GNSS signals. Effectively addressing these challenges is a challenge for the current generation of GNSS algorithms, such as Kalman filtering. When the model becomes unstable or noisy, these limitations may cause diffusion of the estimated positions, which could lead to inaccurate tracking. Furthermore, current algorithms might not always be flexible enough to deal with erratic or noisy situations. High computational complexity, irregular sampling rates among different sensors, and problems with tracking sensitivity and signal acquisition can all impair the performance of GNSS receivers. Therefore, the challenge is to develop more reliable, flexible, and effective GNSS algorithms and methods that can handle these real-world obstacles. It necessitates creative ways to apply advanced mathematical tools like singular value decomposition (SVD) and the Mahalanobis distance concept and apply hybrid optimization techniques. The objective is to develop GNSS tracking systems that can sustain high precision even in difficult situations and are not only accurate but also flexible enough to adjust to changing surroundings.

3. Proposed methodology

The goal of the research is to improve the Extended Adaptive Strong Kalman Filter (EASTKF) algorithm, which will improve GNSS receiver performance in difficult situations. This will be accomplished by utilizing hybrid optimization techniques to build a GNSS system that is more adaptable and resilient. The first step in the research is to configure the Kalman filter's required parameters. The state covariance matrix, measurement noise covariance, process noise covariance, and initial state estimates are all defined in this way. The Kalman filter cannot operate properly without these parameters. The study presents a novel hybrid optimization algorithm Chimphopper Hybrid Optimization (CHHO) to improve process noise covarience(Q_k) and measurement noise covariance (R_k) and fading factor accuracy. The advantages of the Chimp optimization algorithm (ChoA) and the Grasshopper optimization algorithm (GOA) are combined in this algorithm. This hybrid strategy provides a strong framework for GNSS tracking performance optimization. In order to provide dependable and accurate navigation, positioning, and timing even in challenging environments, the research aims to create an advanced GNSS system that can effectively handle real-world challenges. Figure 1 depicts the general flow of the proposed work.

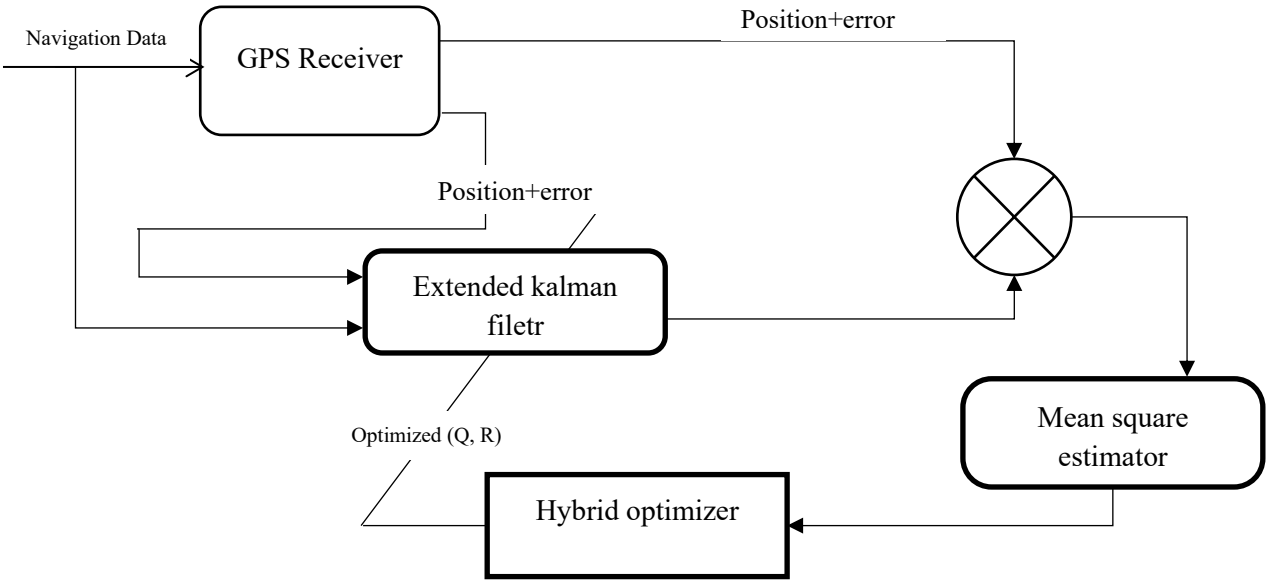

Figure 1. The flow of the proposed work

3.1. GNSS Signal model

A user antenna picks up the GNSS radio frequency (RF) signal. The RF signal is down converted and then converted using analog-to-digital (ADC) technology into a discrete intermediate frequency (IF) signal. An appropriate model for the digital IF signal is

$$r_{IF}(t_s) = A.D(t_s - \tau).C(t_s - \tau).\cos(2\pi(f_{IF} + f_d)\,t_s + \varphi_0) + \omega(t_s) \quad (1)$$

where A is the IF signal amplitude, $D(t_s)$ is the navigation data bit, $C(t_s)$ is the pseudo-random number (PRN) spreading code, τ is the received signal's code delay, and f_{IF} is the intermediate frequency in hertz. The carrier Doppler shift is represented by f_d in hertz, the initial carrier phase is represented by φ_0 in radians, and the additive zero-mean white Gaussian noise (AWGN) is represented by $\omega(t_s)$. To eliminate the carrier frequency, the IF signal is multiplied by two in-phase, 90°-shifted local carriers in every receiver tracking channel. The local code is then multiplied by the final result. The output is then sent to the dump and integration blocks to produce correlated signals for I and Q. I and Q, the prompt branch signals, are characterized as

$$I(k) = A.N(k).R(\tau - \bar{\tau})_k.\frac{\sin(\pi.\delta f(k).T_s)}{\pi.\delta f(k).T_s}.\cos(\overline{\delta\varphi_k}) + \omega_I(k) \quad (2)$$

$$Q(k) = A.N(k).R(\tau - \bar{\tau})_k.\frac{\sin(\pi.\delta f(k).T_s)}{\pi.\delta f(k).T_s}.\sin(\overline{\delta\varphi_k}) + \omega_Q(k) \quad (3)$$

where the correlated values' updated index is denoted by k. The signal amplitude is indicated by A, the total amount of samples that the correlator has gathered is indicated by $N(k)$, and the PRN code's autocorrelation function is shown by $R(\tau - \bar{\tau})_k$. The local prompt PRN code's delay is represented by $\bar{\tau}$; the error in carrier frequency expressed in hertz is represented by $\delta f(k)$; the coherent integration time (CIT) is measured in seconds by T_s; the average carrier phase error over T_s is represented by $\overline{\delta\varphi_k}$; and the white Gaussian noise, both uncorrelated and of equal power, are represented by $\omega_I(k)$ and $\omega_Q(k)$.

3.2. Enhanced Adaptive weighted Strong Tracking Kalman Filter

Initially, the observation model and state space model are defined as

$$X_k = \varphi_{k/k-1} X_{k-1} + \Gamma_{k-1} W_{k-1} \quad (4)$$

$$Y_k = H_k X_k + V_k \quad (5)$$

where X_k and Y_k stand for the dynamic system's state vector and measurement vector, respectively, at discrete time k.The system transition matrix is represented by $\varphi_{\frac{k}{k-1}}$, the observation matrix by H_k, and the system noise assignment matrix byΓ_{k-1} . The statistical characteristics of W_{k-1} and V_k, which are Gaussian white noise sequences with zero-mean and independent for one another, are as follows:

$$E[W_k] = 0 \quad (6)$$

$$E\left[W_k W_j^T\right] = Q_k \gamma_{kj} \quad (7)$$

$$E[V_k] = 0 \quad (8)$$

$$E\left[V_k V_j^T\right] = R_k \gamma_{kj} \quad (9)$$

$$E\left[W_k V_j^T\right] = 0 \quad (10)$$

where the symbol γ for the unit sampling signal in equation (11) is defined as:

$$\gamma_{kj} = \begin{cases} 1 & k = j \\ 0 & k \neq j \end{cases} \quad (11)$$

The prediction and correction process are both parts of the KF iterative mechanism. The method of prediction is as follows:

$$\hat{X}_{k/k-1} = \varphi_{k/k-1} \hat{X}_{k-1} \quad (12)$$

$$P_{k/k-1} = \varphi_{k/k-1} P_{k-1} \varphi_{k/k-1}^T + \Gamma_{k-1} Q_{k-1} \Gamma_{k-1}^T \quad (13)$$

where $\hat{X}_{k/k-1}$ and $P_{k/k-1}$ are the state vector's predicted estimation and covariance matrix, respectively, P_{k-1} and $\hat{X}_{k-1}$ are the covariance matrix and estimated state values, respectively.

$$K_k = P_{k/k-1} H_k^T (H_k P_{\frac{k}{k}-1} H_k^T + R_{k)}^{-1} \quad (14)$$

$$\hat{X}_k = \hat{X}_{k/k-1} + K_k (Y_k - H_k \hat{X}_{k/k-1}) \quad (15)$$

$$P_k = (E - K_k H_k) P_{k/k-1} \quad (16)$$

K_k stands for the Kalman gain.

According to KF, the following defines the innovation sequence equation:

$$\varepsilon_{k/k-1} = Y_k - \hat{Y}_{k/k-1} \quad (17)$$

For the purpose of creating a model that accurately describes the noise and has no model errors, the innovation sequence of the standard KF equation ought to be a zero-mean Gaussian white noise sequence, as shown in the following equation:

$$E[\varepsilon_{k/k-1} \varepsilon_{k/k-1}^T] = H_k \varphi_{k/k-1} P_{k-1} \varphi_{k/k-1}^T H_k^T + H_k \Gamma_{k-1} Q_{k-1} \Gamma_{k-1}^T H_k^T + R_k \quad (18)$$

$$E[\varepsilon_{k/k-1} \varepsilon_{k/k-1}^T] = H_k P_{k/k-1} H_k^T + R_k \quad (19)$$

If there are no significant discrepancies in the system process simulations and noise statistics data, the KF will eventually reach convergence. The availability of a precisely known model, however, is unrealistic in a variety of complex practical situations, and the noise's statistical properties can change significantly because of an unfavourable environment. Due to the mismatch between the system architecture parameter and the noise

description, the balance of (11) will be destroyed. This phenomenon is known as innovation mismatch. The traditional KF method's applications are severely constrained by this drawback. The fundamental goal of STKF is to reduce model or noise parameter errors to levels that are comparable to filter estimation errors. To comply with the orthogonal theory of the innovation sequence, the fading factor is incorporated into the KF process and modifies the predicted error covariance matrix in real-time.

$$E[(x_k - \tilde{x}_k)(x_k - \tilde{x}_k)^T] = min \tag{20}$$

$$E\left[\varepsilon_{k+j}\varepsilon_k^T\right] = 0 \tag{21}$$

Where equation (21) shows that adherence to the prerequisite orthogonal principle is necessary for the innovation sequence and equation (20) indicates the performance assessment indicator for the filter. The predicted error covariance matrix (11) can be rewritten as a result of continuous artificial adjustment.

$$E[\varepsilon_{\frac{k}{k}-1}\varepsilon_{\frac{k}{k}-1}^T] - R_k = H_k(\lambda P_{k/k-1})H_k^T \tag{22}$$

Where λ is the fading factor. The fading factor can be found by computing the trace on both sides of (22) and accounting for the fact that its value should be above one.

$$\lambda_k = \max(1, \frac{tr(N_k)}{tr(M_k)}) \tag{23}$$

$$N_k = V_k - R_k - H_k Q_{k-1}H_k^T \tag{24}$$

$$M_k = H_k P_{k/k-1}H_k^T \tag{25}$$

$$V_k = \begin{cases} \varepsilon_1\varepsilon_1^T & k = 1 \\ \frac{\alpha V_{k-1} + \varepsilon_k\varepsilon_k^T}{1+\alpha}, & k \geq 2 \end{cases} \tag{26}$$

where the forgetting factor, α, has a value between 0 and 1, and the trace operation is tr. The R_k is considered fixed for the STKF during the iteration process. In the variable environments, the inaccurate R_k may have an impact on the accuracy of fading factors.

The two-quadrant arctangent discriminator serves as the carrier phase discriminator for the carrier tracking loop:

$$\Delta\theta_k = \arctan\left(\frac{Q(k)}{I(k)}\right) \tag{27}$$

where $I(k)$ and $Q(k)$ are the correlated signals of inphase and quadrature branch among the received and local signal at the kth epoch, and k is the carrier phase error. The two main sources of measurement error in the carrier tracking loop are dynamic stress error and phase jitter. The output of the arctangent discriminator exhibits (27) noise variance.

$$R_k = \frac{1}{2T(c/n_O)_k}(1 + \frac{1}{2T(c/n_O)_k}) \tag{28}$$

where $\left(\frac{c}{n_O}\right)_k$ is the kth epoch carrier-to-noise power ratio. Moreover, $(c/n_O)_k = 10^{(C/N_O)_{k/10}}$, where $(\frac{C}{N_0})_k$ is in dB- Hz. The $(\frac{C}{N_0})_k$ for GNSS receivers can be predicted based on the signals they receive. Narrowband-wideband power ratio technique (NWPR), which is frequently employed in GNSS receivers, is the foundation of the calculation technique.

The Adaptive Weighted Strong Tracking Kalman Filter (AWSTKF) is intended to handle scenarios in which a dynamic system may experience sudden changes and where the noise characteristics are non-Gaussian. It incorporates a novel idea in this filtering approach: the idea of weighting various measurements according to their importance or reliability.

$$s_i^w = H_{i,k}\hat{X}_{k/k-1} - a_i \tag{29}$$

Where the weighted measurement residual for the *i*-th measurement at time k is represented by the s_i^w. The measurement matrix for the *i*-th measurement is H_k and the actual measurement is a_i. The difference between the expected measurement based on the expected state $(H_{i,k})$and the actual measurement $(a_i)$is essentially the weighted residual. For every measurement, it measures the degree to which the actual measurement and the predicted state agree. As the weighted residual rises, the weight falls, suggesting that measurements with lower levels of reliability are given lower weights.

$$w_k = \exp\left(-\frac{1}{2}\ (s_i^w)^T\ R_{i,k}^{-1}(s_i^w)\right) \quad (30)$$

Where w_i is the weight for the i th measurement. The weight w_k is derived from the exponential of the negative half of the Mahalanobis distance. This gives the number of standard deviations that separate the weighted residual from the measurement residuals' expected value, or mean. When compared to the expected state, it gives an indication of how consistent or reliable the measurement is.

$$K_k = P_{k/k-1\ *}\ w_k *\ H_k^T(H_k P_{\frac{k}{k}-1}\ H_k^T + R_{k)}\ ^{-1} \quad (31)$$

The Kalman gain is weighted by w_k, which incorporates the measurement reliability information. The amount by which the state estimate needs to be modified on the basis of the measurements is determined by the Kalman gain, which functions essentially as a correction factor.

3.3. Chimphopper Hybrid optimization to fine tune R_k

A special fusion of the Grasshopper Optimization Algorithm (Grasshopper), the Chimpanzee Optimization Algorithm (Chimp), and gravitational force principles is the hybrid optimization algorithm presented here. This hybrid optimization approach integrates concepts of gravitational force and chimpanzee and grasshopper behavior to solve complex optimization problems.

Step 1: Initialization

Initialize the necessary parameters such as initial state estimates, state covariance matrix, process noise covariance, and measurement noise covariance.

Step 2: Random generation

Generate the random vectors in the interval [0,1]. In order to introduce randomness into the optimization process, a "chaotic_value" is generated.

Step 3: Fitness function

$$Fitness = optimize(R) \quad (32)$$

Step 4: Exploration phase (Driving and Chasing the Prey)

The hunting of the prey occurs during the phases of exploitation and exploration. Eqs. (33) and (34) are used to computationally replicate driving and pursuing the prey.

$$d = \left|c.z_{prey}(t) - m.z_{chimp}(t)\right| \quad (33)$$

$$z_{chimp}(t+1) = z_{prey}(t) - a.d \quad (34)$$

z_{prey} is the vector of the prey's position, z_{chimp} is the vector of a chimp's position, there are *t* iterations in total. The coefficient vectors are a, m, and c and are computed using Equations (3), (4), and (5),

$$a = 2.f.rand_1 - f \quad (35)$$

$$c = 2.rand_2 \quad (36)$$

$$m = chaotic\_value \quad (37)$$

where, during the iteration process (both in the exploration and exploitation phases), f reduces non-linearly from 2.5 to 0. The random vectors in the interval [0,1] are $rand_1$ and $rand_2$. The chimps' new positions are calculated from their interactions with the prey, in which the chimp attempts to move closer to the prey's location.

Step 5: Attacking Method (Exploitation Phase)

The chimps are able to locate their prey by driving, blocking, and pursuing it before encircling it. Attacking chimps are typically the ones who carry out the hunting process. Chimpanzees that function as barriers, chasers, and drivers occasionally take part in the hunting process. Assuming that the attacker, driver, barrier, and chaser have more knowledge about the target's location, the first solution is assumed to be available in this scenario. Four more optimal solutions that have been found so far are saved for the following iteration, and the remaining chimps are compelled to adjust their own locations in accordance with the best chimp locations. The following mathematical equations (6)– (9) have been used to illustrate this process:

$$d_{attacker} = |c_1 z_{attacker} - m_1 z| \quad (38)$$

$$d_{barrier} = |c_2 z_{barrier} - m_2 z| \quad (39)$$

$$d_{chaser} = |c_3 z_{chaser} - m_3 z| \quad (40)$$

$$d_{driver} = |c_3 z_{driver} - m_4 z| \quad (41)$$

A chimp's next location can be anywhere between its current location and the target's or prey's location if the random vectors fall within the range of [−1, 1]

$$z_1 = z_{attacker} - a_1 . d_{attacker} \quad (42)$$

$$z_2 = z_{barrier} - a_2 . d_{barrier} \quad (43)$$

$$z_3 = z_{chaser} - a_3 . d_{chaser} \quad (44)$$

$$z_4 = z_{driver} - a_4 . d_{driver} \quad (45)$$

The chimps' positions are updated in accordance with their individual roles and interactions with the prey. Equation (14) updates the positions of the chimps during the search process based on the overall equations.

$$z(t+1) = \frac{z_1 + z_2 + z_3 + z_4}{4} \quad (46)$$

Step 6: Gravitational Force based Position Update

The chimp positions are further updated using equations involving a concept of gravitational force derived from the behavior of grasshoppers.

$$z(t+1) = \frac{z_1 + z_2 + z_3 + z_4}{4} * G_i \quad (47)$$

Where G_i is the grasshopper's gravitational force.

$$G_i = -g\hat{e}_g \quad (48)$$

$\hat{e}_g$ is a unit vector toward the earth's center and g is the gravitational constant.

Step 7: Randomized Location Update

Finally, the following mathematical equation has been applied to update the chimp location during the search process in the search domain:

$$z_{chimp}(t+1) = \begin{cases} z_{prey}(t) - a.d & if\ \mu < 0.5 \\ chaotic\_value & if\ \mu > 0.5 \end{cases} \quad (49)$$

Where μ is a random number between [0,1].

Step 8: Save the best solution so far.

Step 9: Terminate.

Chimphopper Hybrid Optimization consists of both the exploration and exploitation stages, in which chimpanzees learn to hunt and attack prey while taking chaotic and random factors into consideration. The optimization process gains additional diversity and adaptability with the application of gravitational force. This strategy makes use of the collective intelligence of chimpanzees, the agility of grasshoppers, and the force of gravity to find superior solutions for difficult optimization problems. A robust foundation for GNSS tracking performance optimization is offered by this hybrid approach.

4. Result and Discussion

The performance of the proposed Enhanced Adaptive Strong Tracking Kalman Filter (E-ASTKF) method is thoroughly evaluated and analysed in the context of tracking the positions X, Y, and Z for a GNSS receiver. This evaluation involves a comparison with several existing techniques, including Least Squares (LS), Kalman Filter (KF), Extended Kalman Filter (EKF), and Adaptive Strong Kalman Filter. To assess the effectiveness of the E-ASTKF method, several performance metrics like MAE (Mean Absolute Error), RMSE (Root Mean Squared Error), MSE (Mean Squared Error), MARE (Mean Absolute Relative Error), MAPE (Mean Absolute Percentage Error), and NMSE (Normalized Mean Squared Error). are used, which encompass a comprehensive understanding of the tracking accuracy. The evaluation is conducted using MATLAB, which facilitates the implementation and analysis of the proposed E-ASTKF method. The performance measures are systematically compared across different algorithms for the X, Y, and Z positions.

4.1. Performance metrics

(i) MAE

The MAE measures the absolute disparities between the anticipated and actual values. The calculation involves dividing the total number of observations by the total amount of absolute differences. The MAE metric is a reliable indicator of outlier presence in data because it consistently has a positive value.

$$MAE = \frac{1}{n}\sum_{i=1}^{n}|Y - Y'|^2 \tag{50}$$

(ii) RMSE

The RMSE of a dataset is the average squared difference between the observed and predicted values. It is determined by taking the squared differences between the expected and actual values and averaging them.

$$RMSE = \sqrt{\frac{1}{n}\sum_{i=1}^{n}|Y - Y'|^2} \tag{51}$$

(iii) MSE

The MSE represents the mean of the squared deviations between the observed and predicted values. It is not square root based, but it is similar to RMSE.

$$MSE = \frac{1}{n}\sum_{i=1}^{n}(Y - Y')^2 \tag{52}$$

(iv) MAPE

The MAPE computes the percentage that separates the expected value from the actual value. It is calculated using the absolute percentage variation in the mean of the observed and predicted values.

$$MAPE = \frac{1}{n}\sum_{i=1}^{n}\left|\frac{Y-Y'}{Y}\right| \times 100 \tag{53}$$

(v) MARE (Mean Absolute Relative Error)

MARE is calculated by dividing the average of the actual values by the average of the absolute variations between the actual and predicted values.

$$MARE = \frac{1}{n}\sum_{i=1}^{n}\left|\frac{Y-Y'}{Y}\right| \tag{54}$$

(vi) NMSE (Normalized Mean Squared Error).

NMSE is the name of a scaled version of MSE. The MSE to variance of the actual values ratio is used to calculate it.

$$NMSE = \frac{1}{n}\sum_{i=1}^{n}\frac{(Y-Y\prime)^2}{VAR(Y)} \quad (55)$$

Where n = number of data points

Y = actual value

Y' = predicted value

4.2. Performance analysis

The performance analysis for different metrics is conducted by comparing and evaluating several existing algorithms, including LS, KF, EKF, PSO-KF and the proposed algorithm (E-ASTKF). This evaluation is carried out for tracking performance in three distinct positions: X, Y, and Z. The outcomes of this evaluation are presented in three separate tables, labelled as Table 1, Table 2, and Table 3, each corresponding to one of these positions.

Table 1. Comparison table for X position

	X- Position					
	MAE	RMSE	MSE	MARE (E =10^{-5})	MAPE	NMSE (E=10^{-10})
Proposed	5.51778	7.11101	50.5665	4.12E-06	0.00041	2.82E-11
PSO-KF	11.8846	13.5767	184.326	8.88E-06	0.00089	1.03E-10
EKF	21.7878	22.834	521.389	1.63E-05	0.00163	2.91E-10
KF	23.2988	24.2543	588.27	1.74E-05	0.00174	3.29E-10
LS	32.2903	32.9389	1084.97	2.41E-05	0.00241	6.06E-10

Table 2. Comparison table for Y position

	Y- Position					
	MAE	RMSE	MSE	MARE (E =10^{-6})	MAPE	NMSE (E=10^{-11})
Proposed	8.32897	11.2667	126.94	1.37E-06	0.00014	3.44E-12
PSO-KF	10.4008	12.4448	154.874	1.71E-06	0.00017	4.20E-12
EKF	17.3562	19.5813	383.426	2.86E-06	0.00029	1.04E-11
KF	23.5827	25.8095	666.133	3.88E-06	0.00039	1.81E-11
LS	24.9943	27.0873	733.723	4.12E-06	0.00041	1.99E-11

Table 3. Comparison table for Z position

	Z- Position					
	MAE	RMSE	MSE	MARE	MAPE	NMSE

				(E =10^{-5})		(E=10^{-10})
Proposed	5.12147	6.10303	37.247	3.59E-06	0.00036	1.83E-11
PSO-KF	16.315	16.9002	285.618	1.14E-05	0.00114	1.40E-10
EKF	18.6767	19.1819	367.947	1.31E-05	0.00131	1.80E-10
KF	22.6485	23.1484	535.849	1.59E-05	0.00159	2.63E-10
LS	26.2096	27.6958	767.055	1.84E-05	0.00184	3.76E-10

(i) MAE

The results of the proposed and current models of MAE for three distinct places are shown in Figure 3.

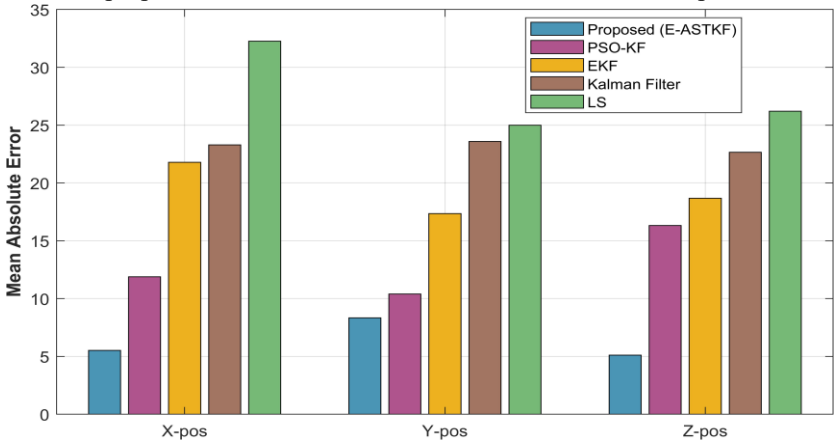

Figure 3. MAE analysis

In all three dimensions, the proposed tracking algorithm—designated as E-ASTKF—shows the best tracking accuracy with the lowest MAE values. It estimates the East-West position with high precision, as evidenced by the X-Pos MAE of 5.52, whereas the Z-Pos (5.12) and Y-Pos (8.33) Additionally, MAE values exhibit impressive vertical and North-South positioning accuracy. The proposed E-ASTKF algorithm performs better than other algorithms in terms of the accuracy of GNSS receiver tracking, especially when it comes to East-West positioning. The tracking performance of the PSO-KF, EKF, and KF approaches is intermediate, while the MAE values of the LS approach are relatively higher.

(ii) RMSE

Figure 4 shows the RMSE outcome of the proposed and existing models for three different positions. In every dimension, the proposed tracking algorithm, E-ASTKF, shows a comparatively low RMSE. With an RMSE of 7.11, it shows particularly good accuracy in the East-West direction (X-Pos), indicating accurate horizontal positioning. The RMSE values for Y-Pos (11.27) and Z-Pos (6.10) indicate strong accuracy in both vertical and North-South positioning. Compared to other algorithms, the proposed E-ASTKF algorithm provides superior tracking accuracy with notably accurate East-West positioning. In particular, the vertical dimension exhibits reduced accuracy when compared to the PSO-KF, EKF, and KF methods. With a moderate tracking accuracy, the LS method lies in the middle of the two extremes.

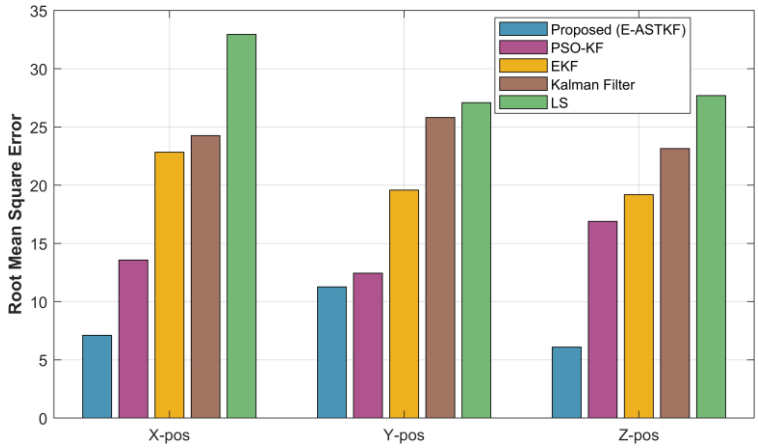

Figure 4. RMSE analysis

(iii) MSE

Figure 5 shows the MSE outcome of the proposed and existing models for three different positions.

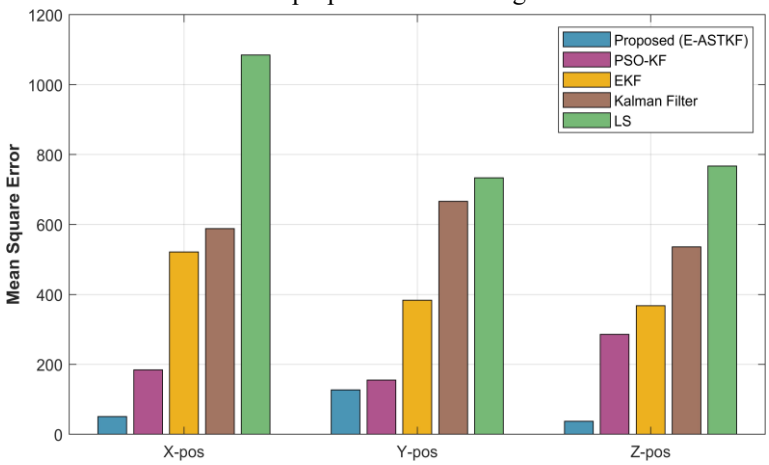

Figure 5. MSE analysis

The proposed E-ASTKF tracking algorithm, has the highest tracking accuracy as it shows the lowest MSE across all three dimensions. With an MSE of 50.57, it performs exceptionally well in East-West positioning (X-Pos), demonstrating accurate horizontal tracking. Strong accuracy in North-South and vertical positioning is also demonstrated by the MSE values for Y-Pos (126.94) and Z-Pos (37.25). The best tracking accuracy, particularly in East-West positioning, is provided by the proposed E-ASTKF algorithm, which performs better than alternative algorithms. The LS method performs in an intermediate manner compared to the PSO-KF, EKF, and KF methods, which show lower tracking accuracy.

(iv) MAPE

The results of the proposed and current models of MAPE for three distinct places are depicted in Figure 6.

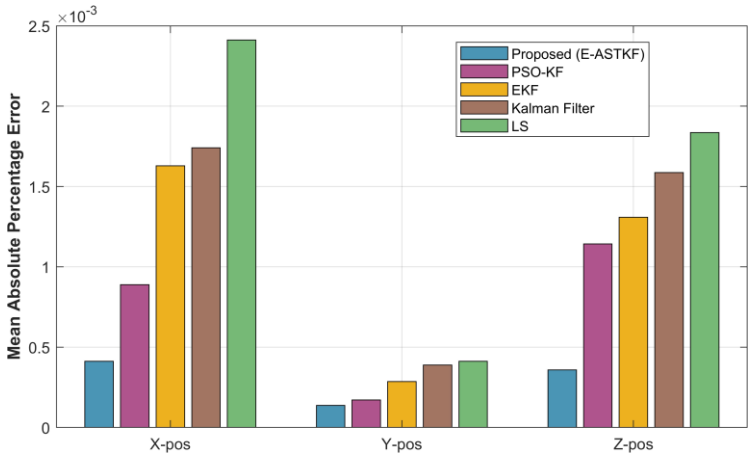

Figure 6. MAPE analysis

The low MAPE values are shown by the proposed tracking algorithm, E-ASTKF, in all three dimensions, indicating excellent tracking accuracy. It performs exceptionally well in East-West positioning (X-Pos) with a MAPE of 0.00041241, which corresponds to very accurate horizontal tracking. Furthermore, the MAPE values for Z-Pos (0.000358677) and Y-Pos (0.000137208) show its exceptional accuracy in vertical and North-South positioning. LS method performs in an intermediate manner; PSO-KF, EKF, and KF methods, on the other hand, show lower accuracy.

(v) MARE

Figure 7 displays the outcomes of the proposed and existing MARE models for three different locations.

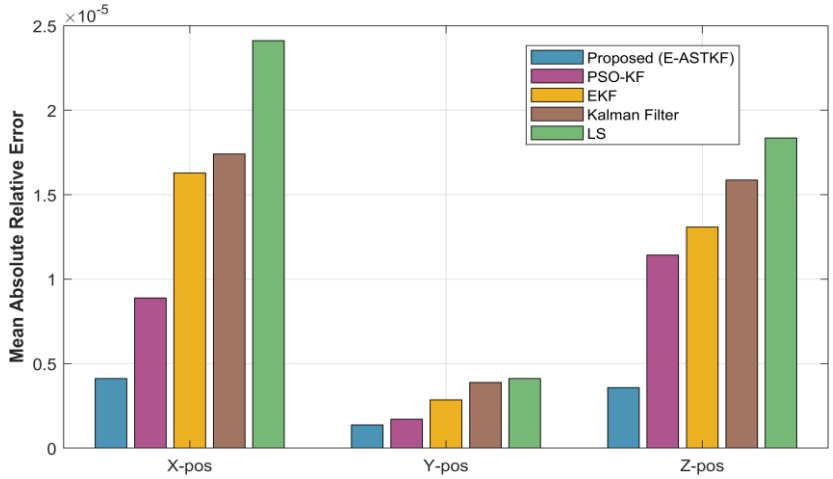

Figure 7. MARE analysis

Among all the approaches, the Proposed (E-ASTKF) algorithm provides the best tracking performance with the least amount of position errors. With X, Y, and Z position errors in the range of 10^{-6}, it achieves striking precision. This shows that the suggested algorithm is very good at reducing tracking errors and may be appropriate for uses like autonomous navigation systems or geodetic surveying which utilize for highly accurate GNSS positioning.

(vi) NMSE

The results of the proposed and current models of NMSE for three distinct places are depicted in Figure 8.

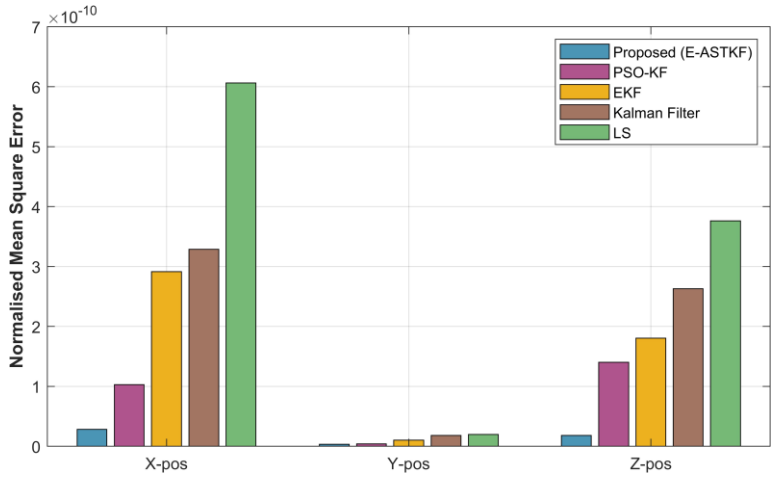

Figure 8. NMSE analysis

The proposed tracking algorithm, E-ASTKF, exhibits an exceptional degree of tracking accuracy with incredibly low NMSE values across all three dimensions. This indicates very good tracking accuracy, especially in East-West (X-Pos) positioning (NMSE = 2.82E-11). The Y-Pos (3.44E-12) and Z-Pos (1.83E-11) NMSE values highlight the system's exceptional accuracy in vertical and North-South positioning.

4.3. Error positions of the proposed and the exisiting

This section examines the error positions with respect to time epoch for a number of existing algorithms, such as LS, KF, and EKF, as well as the proposed algorithm, E-ASTKF. With the GPS satellite constellation being dynamic and their orbits changing over time, this analysis aims at understanding how GPS positioning errors can change over time. Epoch time and error positioning have a significant correlation that emphasizes the temporal dimension of GNSS tracking accuracy. The constellation of GPS satellites is constantly changing in terms of composition and geometry as they travel through space. This dynamic quality may have an impact on GNSS receiver positioning accuracy. As the receiver interacts with various satellite signals, errors may differ between epochs. Figures 9, 10, 11, 12 and 13 are graphical insights into the error positions associated with LS, KF, EKF, ASTKF, and the proposed E-ASTKF algorithm, respectively.

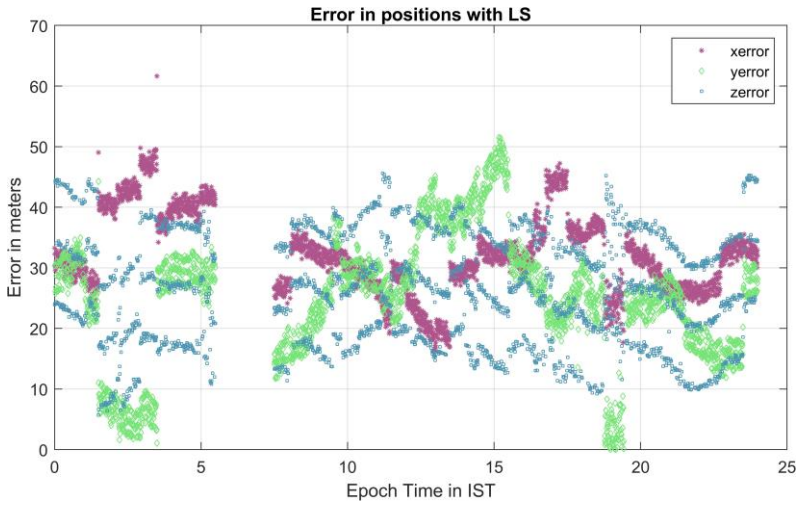

Figure 9. Error position in LS

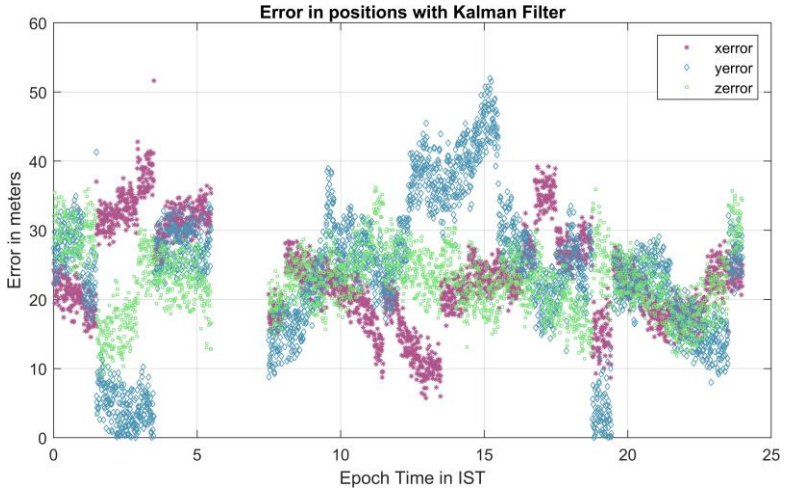

Figure 10. Error position in KF

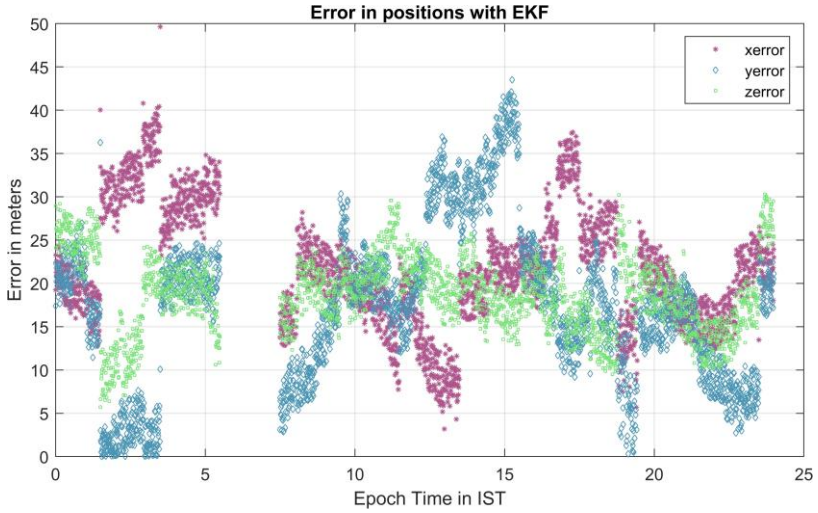

Figure 11. Error position in EKF

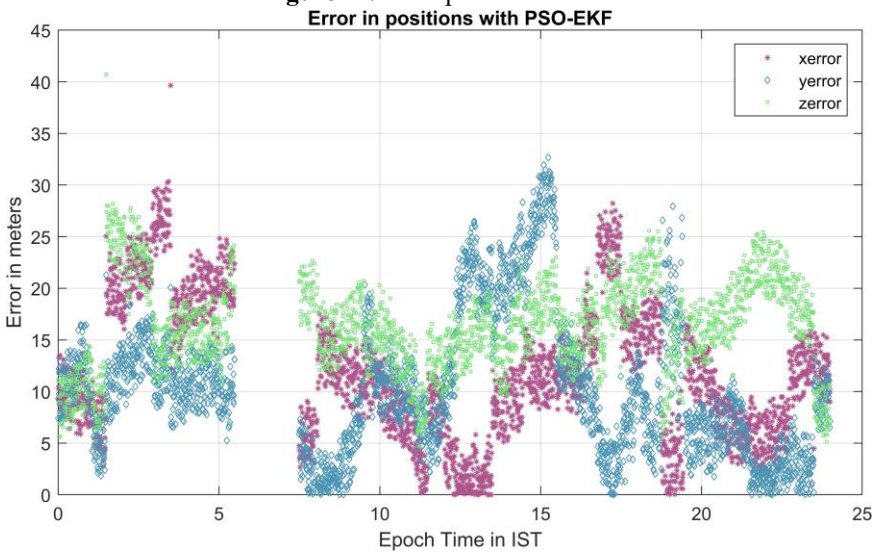

Figure 12. Error position in PSO- EKF

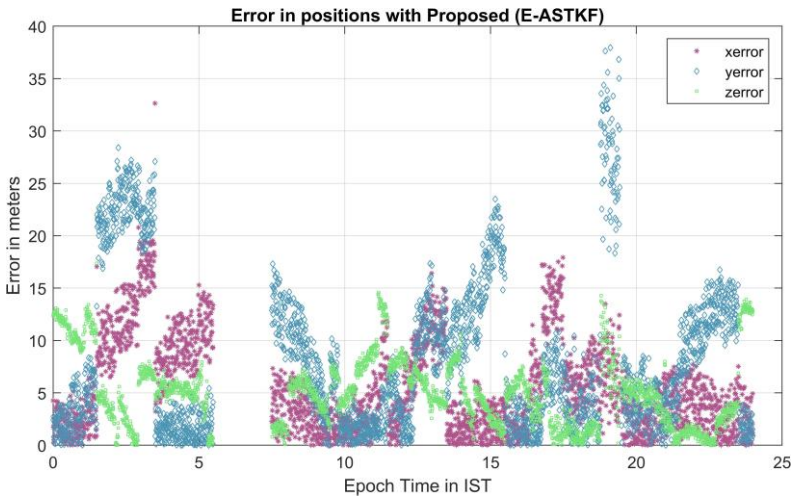

Figure 13. Error position in E-ASTKF

From the position errors graph, the proposed method has the lowest error in position for the various time epoch compared to the existing approaches. Hence the proposed PSO-EKF outperforms the other algorithms in terms of position error.

5. Conclusion

The novel Chimphopper Hybrid Optimization (CHHO) technique, combined with the enhanced Adaptive Strong Extended Kalman Filter (E-ASTKF) algorithm, was created and extensively tested to improve GNSS system performance. The main goal was to develop a more resilient and versatile GNSS receiver that could provide precise location and navigation even in the face of difficult circumstances like dynamic movement, varying noise statistics, and weak signal reception. The findings of this research show that, in comparison to other methods such as LS, KF, EKF and PSO-KF, the E-ASTKF, considerably improves GNSS receiver accuracy. The E-ASTKF approach is superior, as evidenced by the performance metrics used, which include MAE, RMSE, MSE, MARE, MAPE, and NMSE. This work addresses real-world navigation and positioning challenges and is a promising step towards more robust and reliable GNSS systems. Through the combination of modern optimization methods with the conventional Kalman filter approach, the study creates a strong synergy that allows GNSS receivers to function well in challenging environments. The results of this research could be useful for many different applications, such as emergency response systems, geospatial surveying, autonomous cars, and precision agriculture. The proposed E-ASTKF technique greatly increase GNSS receiver accuracy and reliability, resulting in safer and more effective positioning and navigation in challenging environments.

References

1. Murray, J.R., Bartlow, N., Bock, Y., Brooks, B.A., Foster, J., Freymueller, J., Hammond, W.C., Hodgkinson, K., Johanson, I., López-Venegas, A. and Mann, D., 2020. Regional global navigation satellite system networks for crustal deformation monitoring. *Seismological Research Letters*, *91*(2A), pp.552-572.
2. Cao, S., Lu, X. and Shen, S., 2022. GVINS: Tightly coupled GNSS–visual–inertial fusion for smooth and consistent state estimation. *IEEE Transactions on Robotics*, *38*(4), pp.2004-2021.
3. Cortés, I., Conde, N., Van Der Merwe, J.R., Lohan, E.S., Nurmi, J. and Felber, W., 2022, June. Low-complexity adaptive direct-state Kalman filter for robust GNSS carrier tracking. In *2022 International Conference on Localization and GNSS (ICL-GNSS)* (pp. 1-7). IEEE.
4. Luo, Z., Ding, J. and Zhao, L., 2018. Adaptive gain control method of a phase-locked loop for gnss carrier signal tracking. *International Journal of Antennas and Propagation*, *2018*.
5. Yang, R., Huang, J., Zhan, X. and Luo, S., 2021. Decentralized FLL-Assisted PLL design for robust GNSS carrier tracking. *IEEE Communications Letters*, *25*(10), pp.3379-3383.
6. Elghamrawy, H., Karaim, M., Tamazin, M. and Noureldin, A., 2020. Experimental evaluation of the impact of different types of jamming signals on commercial GNSS receivers. *Applied Sciences*, *10*(12), p.4240.

7. Liu, G. and Wang, L., 2022. Joint Tracking GPS and Leo Signals with Adaptive Vector Tracking Loop in Challenging Environments. *The International Archives of the Photogrammetry, Remote Sensing and Spatial Information Sciences*, *46*, pp.119-124.
8. Deng, X., Deng, Z., Liu, J. and Zhang, Z., 2022. A Novel Carrier Loop Based on Coarse-to-Fine Weighted Adaptive Kalman Filter for Weak Communication-Positioning Integrated Signal. *Sensors*, *22*(11), p.4068.
9. Wu, F., Luo, H., Jia, H., Zhao, F., Xiao, Y. and Gao, X., 2020. Predicting the noise covariance with a multitask learning model for Kalman filter-based GNSS/INS integrated navigation. *IEEE Transactions on Instrumentation and Measurement*, *70*, pp.1-13.
10. Fan, P., Cui, X., Zhao, S., Liu, G. and Lu, M., 2021. A two-step stochastic hybrid estimation for GNSS carrier phase tracking in urban environments. *IEEE Transactions on Instrumentation and Measurement*, *70*, pp.1-18.
11. Chang, Y., Wang, Y., Shen, Y. and Ji, C., 2021. A new fuzzy strong tracking cubature Kalman filter for INS/GNSS. *GPS Solutions*, *25*(3), p.120.
12. Tang, X., Chen, X., Pei, Z. and Wang, P., 2019. The explicit tuning investigation and validation of a full Kalman filter-based tracking loop in GNSS receivers. *IEEE Access*, *7*, pp.111487-111498.
13. Chiang, K.W., Tsai, G.J., Chu, H.J. and El-Sheimy, N., 2020. Performance enhancement of INS/GNSS/Refreshed-SLAM integration for acceptable lane-level navigation accuracy. *IEEE Transactions on Vehicular Technology*, *69*(3), pp.2463-2476.
14. Zhang, A., Shuida, B.A.O., Fei, G.A.O. and Wenhao, B.I., 2019. A novel strong tracking cubature Kalman filter and its application in maneuvering target tracking. *Chinese Journal of Aeronautics*, *32*(11), pp.2489-2502.
15. Cheng, Y. and Chang, Q., 2020. A carrier tracking loop using adaptive strong tracking Kalman filter in GNSS receivers. *IEEE Communications Letters*, *24*(12), pp.2903-2907.
16. Sun, B., Zhang, Z., Liu, S., Yan, X. and Yang, C., 2022. Integrated Navigation Algorithm Based on Multiple Fading Factors Kalman Filter. *Sensors*, *22*(14), p.5081.
17. Yue, Z., Lian, B., Tong, K. and Chen, S., 2019. Novel strong tracking square-root cubature Kalman filter for GNSS/INS integrated navigation system. *IET Radar, Sonar & Navigation*, *13*(6), pp.976-982.
18. Pan, C., Qian, N., Li, Z., Gao, J., Liu, Z. and Shao, K., 2021. A robust adaptive cubature Kalman filter based on SVD for dual-antenna GNSS/MIMU tightly coupled integration. *Remote Sensing*, *13*(10), p.1943.
19. Lou, T.S., Chen, N.H., Chen, Z.W. and Wang, X.L., 2019. Robust partially strong tracking extended consider Kalman filtering for INS/GNSS integrated navigation. *IEEE Access*, *7*, pp.151230-151238.
20. Shen, C., Xiong, Y., Zhao, D., Wang, C., Cao, H., Song, X., Tang, J. and Liu, J., 2022. Multi-rate strong tracking square-root cubature Kalman filter for MEMS-INS/GPS/polarization compass integrated navigation system. *Mechanical Systems and Signal Processing*, *163*, p.108146.
21. Liu, S., Li, S., Zheng, J., Fu, Q. and Yuan, Y., 2020. C/N0 Estimator Based on the Adaptive Strong Tracking Kalman Filter for GNSS Vector Receivers. *Sensors*, *20*(3), p.739.
22. Mu, R. and Long, T., 2021. Design and implementation of vector tracking loop for high-dynamic gnss receiver. *Sensors*, *21*(16), p.5629.
23. Gao, B., Hu, G., Zhong, Y. and Zhu, X., 2021. Cubature Kalman filter with both adaptability and robustness for tightly-coupled GNSS/INS integration. *IEEE Sensors Journal*, *21*(13), pp.14997-15011.
24. Cheng, L., Dai, Y., Guo, W. and Zheng, J., 2021. Structure and performance analysis of signal acquisition and Doppler tracking in LEO augmented GNSS receiver. Sensors, 21(2), p.525.
25. Klokov, A., Kanouj, M. and Mironchev, A., 2022. A novel carrier tracking approach for GPS signals based on Gauss–Hermite Kalman filter. Electronics, 11(14), p.2215.